Journal of Materials Chemistry C

ROYAL SOCIETY OF CHEMISTRY

PAPER

View Article Online
View Journal | View Issue

Open Access Article. Published on 08 August 2024. Downloaded on 10/19/2025 2:20:13 PM.
This article is licensed under a Creative Commons Attribution 3.0 Unported Licence.

Check for updates

Cite this: J. Mater. Chem. C, 2024, 12, 14658

Designing the thermal processing of $Ba(Ti_{0.8}Zr_{0.2})O_3$–$(Ba_{0.7}Ca_{0.3})TiO_3$ thin films from an ethylene glycol-derived precursor

Sabi William Konsago,*[ab] Katarina Žiberna,[ab] Jernej Ekar,[ab] Janez Kovač[ab] and Barbara Malič*[ab]

Received 14th June 2024,
Accepted 8th August 2024

DOI: 10.1039/d4tc02495h

rsc.li/materials-c

Lead-free ferroelectric $0.5Ba(Ti_{0.8}Zr_{0.2})O_3$–$0.5(Ba_{0.7}Ca_{0.3})TiO_3$ (BZT–BCT) thin films on platinized silicon substrates are prepared by a chemical solution deposition route. The solution chemistry involves the use of ethylene glycol and ethanol as solvents for alkaline earth acetates and transition metal alkoxides, respectively. The thermal decomposition of the BZT–BCT xerogel, the crystallization process of BZT–BCT thin films, and their homogeneity are investigated. In the xerogel, the decomposition of the organic residues occurs between 290 °C and 514 °C, followed by the formation of carbonate groups and their decomposition between 580 °C and 775 °C. In the thin films, the sequence of drying and pyrolysis steps, and the concentration of the coating solution influence the formation of carbonate groups and their decomposition upon annealing. Extending the drying and pyrolysis times from 2 minutes to 15 minutes and lowering the concentration of the coating solution from 0.2 M to 0.1 M contribute to an easier thermal decomposition of the carbon residues. Time-of-flight secondary ion mass spectrometry analysis reveals that upon rapid thermal annealing, the decomposition of the carbonate residues in a few tens of nanometres thick BZT–BCT film proceeds from the top downwards, resulting in a pure perovskite phase faster in the thinner films than in thicker ones. The about 100 nm thick BZT–BCT film annealed at 850 °C exhibits a columnar microstructure with a homogeneous distribution of elements across the thickness of the film.

Introduction

Barium zirconate titanate–barium calcium titanate ($Ba(Ti_{0.8}Zr_{0.2})O_3$–$(Ba_{0.7}Ca_{0.3})TiO_3$, BZT–BCT) with an approximately equimolar ratio of BZT to BCT has been recently intensively studied due to the discovery of its large piezoelectric response as a lead-free alternative to lead-based materials in applications.[1–4] The origin of the large piezoelectric response in this material has been essentially explained by its chemical composition and the multiphase coexistence.[1,5–8] A high polarization and a low coercive field, in addition to large piezoelectric coefficients, indicate the multifunctionality of BZT–BCT as an attractive material for potential piezoelectric and energy storage applications.[9] The design of actuators, sensors, transducers, *etc.* for nanoelectromechanical systems (NEMS) requires a small-scale size of the functional material where the materials are used in the thin film form.[10,11]

For the successful design of thin film microstructures and properties, especially using chemical solution deposition (CSD), which presents some advantages over physical vapor deposition methods, including low-cost investment, the control of stoichiometry, fast processing, and uniform surface coverage over large areas, it is critical to control the chemistry of the coating solution, and understand the thermal decomposition process of the deposited film and the film–substrate interaction upon heating. Such detailed studies of the decomposition process, crystallization, and distribution of elements in BZT–BCT thin films by CSD are still missing.

Barium titanate ($BaTiO_3$, BT) is the reference material for studying the processing and properties of BT-based compositions such as BZT–BCT. In CSD, following the conventional method using carboxylic acids, mainly acetic acid, and alcohols as solvents for barium carboxylates and titanium alkoxides, respectively,[12] the perovskite BT phase is formed through oxycarbonate intermediate phases, and temperatures above 650 °C are needed to decompose carbon residues.[12–14] The persistence of carbon residues in CSD-derived BT thin films, even at temperatures up to 1000 °C, has been reported.[15,16] Varying the solution chemistry and optimizing the processing conditions could contribute to lowering the decomposition temperatures of (oxy-)carbonate groups in BT-based films. We reported a new CSD route for BT thin films using

[a] Jožef Stefan Institute, Jamova cesta 39, 1000 Ljubljana, Slovenia. E-mail: sabi.william.konsago@ijs.si, barbara.malic@ijs.si
[b] Jožef Stefan International Postgraduate School, Jamova cesta 39, 1000 Ljubljana, Slovenia

 This journal is © The Royal Society of Chemistry 2024

Open Access Article. Published on 08 August 2024. Downloaded on 10/19/2025 2:20:13 PM.
This article is licensed under a Creative Commons Attribution 3.0 Unported Licence.

ethylene glycol (EG) and ethanol (EtOH) as solvents, in which the carbonate decomposition is concluded at about 600 °C as evidenced by Fourier transform infrared (FTIR) spectroscopy.[17] Furthermore, the BT coating solution prepared using the combination of EG–EtOH solvents is stable for several months.

In the process of BZT–BCT film crystallization, in addition to barium oxycarbonate as an intermediate, we expect calcium oxycarbonate to form as well. Similar to barium carbonate, the decomposition of calcium carbonate requires high temperatures of 765–790 °C.[18,19] Zirconium alkoxides are more reactive than their titanium counterparts due to the lower electronegativity and larger coordination number of the former ion. The electronegativity values (Pauling scale) of titanium and zirconium are 1.54 and 1.33.[20,21] The coordination numbers of respective elements in *n*-alkoxides are 5 and 6, respectively,[22,23] and they could react with other constituents of the coating solution differently. Four cations in the solid solution make the control of the solution chemistry, crystallization, microstructure, and homogeneity of the BZT–BCT films very challenging.

The commonly reported microstructure of CSD-derived BZT–BCT thin films, prepared by the conventional carboxylic acid-based route with thicknesses of up to a few 100 nm consists of fine equiaxed grains with sizes of about 10 nm to a few 10 nm, intergranular pores and cracks.[24–26] In an attempt to control the microstructure of BZT–BCT films, barium metal, calcium nitrate, and transition metal alkoxides were introduced as reagents, but secondary phases in the films were reported.[27] It was speculated that the secondary calcium-zirconium-oxide phase is formed in a BZT–BCT film on a Si-substrate prepared by a conventional carboxylic acid-based CSD route and annealed at 800 °C due to the diffusion of Ca and Zr from the perovskite phase and their consequent reaction with oxygen.[28] Xu *et al.* observed a TiO_2 peak on the XRD pattern of the BZT–BCT film doped with 1 mol% Er^{3+}, with a fine granular microstructure and annealed at 800 °C.[29]

In our previous work, BZT–BCT films with a columnar microstructure with the preferred (111) perovskite orientation were achieved *via* CSD from a 0.1 M coating solution based on an EG–EtOH solvent combination and deposited on platinized silicon substrates using a multistep deposition/annealing process at 850 °C. Doping with manganese (1 mol%) significantly reduced the leakage current and enabled good ferroelectric and piezoelectric properties.[30]

In this work, the thermal processing of BZT–BCT thin films prepared using the above-mentioned solution chemistry is studied. The analysis of the thermal decomposition of the xerogel helped to determine the optimal temperatures of drying, pyrolysis, and annealing. The functional group decomposition and crystallization process in the films, the homogeneity, and distribution of elements across the thickness of selected BZT–BCT thin films are investigated.

Experimental

The $0.5Ba(Ti_{0.8}Zr_{0.2})O_3$–$0.5(Ba_{0.7}Ca_{0.3})TiO_3$ (BZT–BCT) precursor was prepared using barium acetate ($Ba(CH_3COO)_2$ with a purity of 99.97%, Sigma-Aldrich, St. Louis, Missouri, USA), calcium acetate ($Ca(CH_3COO)_2$, 99.999%, Alfa Aesar, Karlsruhe, Germany), titanium *n*-butoxide ($Ti(OC_4H_9)_4$, $Ti(OnBu)_4$), 99.61% and zirconium *n*-butoxide ($Zr(OC_4H_9)_4$ $Zr(OnBu)_4$), 80% both alkoxides purchased from Alfa Aesar, Karlsruhe, Germany are used as reagents. Ethylene glycol ($OHCH_2CH_2OH$, EG, 99.8%) and absolute ethanol (CH_3CH_2OH, EtOH 99.9%) both from Sigma-Aldrich, St. Louis, USA and stored in the dry box, were used to dissolve alkaline earth metal acetates and to dilute transition metal alkoxides, respectively. Both solutions were then mixed at room temperature for 2 hours, with the concentration adjusted to 0.2 M and 0.1 M. All manipulations of reagents were performed in a dry nitrogen atmosphere. The BZT–BCT solutions were stored at 4 °C. The coating solutions are stable for several months. For more details about the synthesis, please refer to our previous study.[30]

The BZT–BCT xerogel was prepared by drying the BZT–BCT solution at 200 °C for 12 h. A thermal analyzer coupled with a mass spectrometer (STA 409, Netzsch + ThermoStar, Balzers Instruments) was used to investigate the thermal decomposition of the gel. The thermogravimetric curve (TG), and the differential thermal analysis (DTA), and evolved gas analysis (EGA) were recorded from room temperature up to 1200 °C in 33.25 mg of BZT–BCT xerogel in a Pt/Rh crucible with a heating rate of 10 K min^{-1} in a flowing synthetic air atmosphere. The rest of the xerogel was calcined at 900 °C and X-ray diffraction (XRD) of the obtained powder was recorded using an X-ray diffractometer (Rigaku MiniFlex 600) with the following parameters: 2 theta = 20–60°, step = 0.034°, time per step = 100 s, soller slit = 0.02, mask10.

BZT–BCT films were deposited by spin coating 0.2 M and 0.1 M BZT–BCT solutions on $Pt(111)/TiO_2/SiO_2/Si(100)$ substrates (Pt/Si, purchased from SINTEF, Oslo, Norway) at 3000 rpm for 30 seconds. The as-deposited films were dried at 250 °C for 2 minutes or 15 minutes and pyrolyzed at 350 °C for 2 minutes or 15 minutes on hot plates. The pyrolysis step was followed by rapid thermal annealing (RTA) in the Mila 5000 furnace (Ulvac-Riko, Yokohama, Japan) at different temperatures with a heating rate of 13.3 °C s^{-1} between 500 °C and 800 °C with the hold-times of 6 seconds. The films consisting of one deposited layer were prepared to study the decomposition process of organics, the formation of carbonates, and their decomposition. For simplification, the following designation is used for these BZT–BCT films:

0.2M-2min: films deposited from the 0.2 M solution with 2 minutes of drying and pyrolysis;

0.2M-15min: films deposited from the 0.2 M solution with 15 minutes of drying and pyrolysis;

0.1M-15min: films deposited from the 0.1 M solution with 15 minutes of drying and pyrolysis.

Within the study of the microstructure and homogeneity, BZT–BCT films were prepared from the 0.2 M and 0.1 M coating solutions by repeating 4 and 10 times, respectively, the deposition/drying at 250 °C for 15 minutes/pyrolysis at 350 °C for 15 minutes/annealing at 600 °C, 700 °C, 800 °C and 850 °C with the same heating rate of 13.3 °C s^{-1}. The first and last layers

Open Access Article. Published on 08 August 2024. Downloaded on 10/19/2025 2:20:13 PM.
This article is licensed under a Creative Commons Attribution 3.0 Unported Licence.

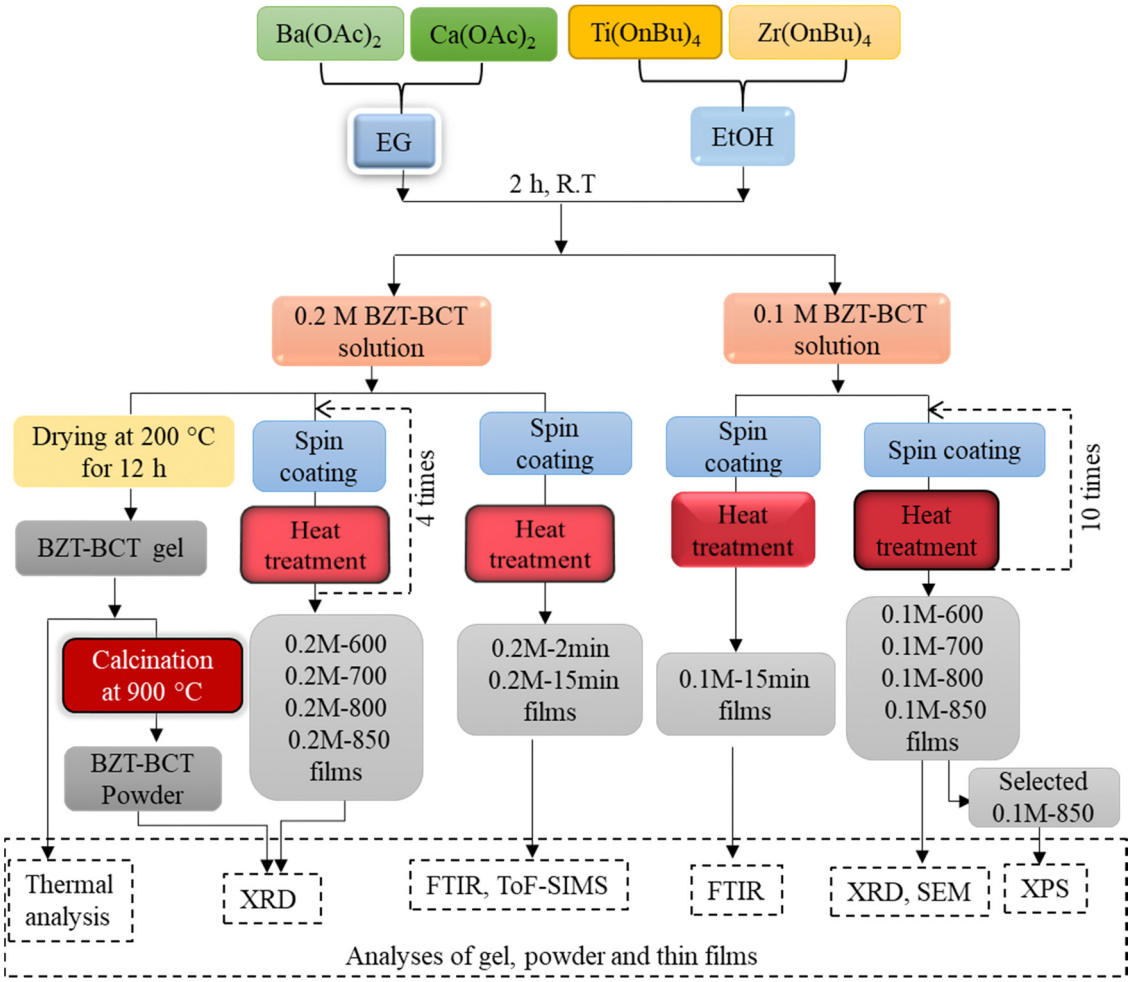

Fig. 1 Schematic description of BZT–BCT solution synthesis, the processing of the gel, powder, thin films and the analyses of the samples.

were annealed for 15 minutes, and the intermediate layers were annealed for 5 minutes at the corresponding temperatures. The films prepared from the 0.2 M and 0.1 M coating solutions are denoted as 0.2M-600, 0.2M-700, 0.2M-800, 0.2M-850, and 0.1M-600, 0.1M-700, 0.1M-800 and 0.1M-850.

One-layer films prepared at different temperatures were analyzed by attenuated total reflectance-Fourier transform infrared spectroscopy (PerkinElmer ATR-FTIR spectrum 100, 4000–380 cm^{-1}).

XRD of the BZT–BCT films were recorded on a high-resolution diffractometer (X'Pert PRO, PANalytical, Almelo, The Netherlands, Cu Kα radiation) using the following parameters: 2 theta = 10–39°, 40–65°, step = 0.034°, time per step = 100 s, soller slit = 0.02, mask10. The X'pert high score plus software for the phase analysis was used to analyze the XRD data.

The microstructure analyses of the films were performed on a field-emission scanning electron microscope (SEM) Verios 4G HP (Thermo Fischer, Waltham, Massachusetts, USA).

Time-of-flight secondary ion mass spectrometry (ToF-SIMS) dual-beam depth profiling was performed on the TOF-SIMS 5 instrument from IONTOF (Münster, Germany). Bi^+ ions were used for the analysis and Cs^+ ions for the depth profiling (crater etching). The energy of the Bi^+ ion beam was 30 keV and the current approximately 1.1 pA. The energy of the Cs^+ ions was 1 keV and the current between 64 and 66 nA. The information depth was around 2 nm and lateral resolution 5 μm. The secondary ions were detected over the *m/z* range from 0 to 800 in the negative polarity. The analytical scanning area was of the size of 100 μm × 100 μm in the center of the Cs-sputtering generated crater of the size of 400 μm × 400 μm. The pressure in the analytical chamber was in the range of 10^{-10} mbar.

The X-ray photoelectron spectroscopy (XPS) analyses were carried out on the PHI-TFA XPS spectrometer produced by Physical Electronics Inc. equipped with an Al-monochromatic source emitting photons at the energy of 1486.6 eV. The analyzed area was 0.4 mm in diameter. Quantification of surface composition was performed from XPS peak intensities taking into account relative sensitivity factors provided by the instrument manufacturer.[31] XPS depth profiling was performed *via* a 3 keV Ar^+ ion beam rastering over an area of 3 × 3 mm with an etching rate of 3.0 nm min^{-1} measured on a Ni/Cr multilayer of known thickness.

Fig. 1 summarizes the procedure for BZT–BCT solution synthesis, the processing of gel, powder, and thin films, and the analyses of individual samples.

Open Access Article. Published on 08 August 2024. Downloaded on 10/19/2025 2:20:13 PM.
This article is licensed under a Creative Commons Attribution 3.0 Unported Licence.

Results and discussion

The thermal decomposition process of the BZT–BCT gel is analyzed by using TG-DTA coupled with EGA, and the results are shown in Fig. 2. A slight weight loss of about 1% from room temperature to about 200 °C observed in the TG curve is accompanied by a weak endothermic peak due to the evaporation of captured moisture by the gel. This evaporation is recorded in the EGA curve at about 100 °C. From 217 °C, we observe a progressive weight loss of 31% accompanied by a series of massive exothermic peaks at 290 °C, 316 °C, 410 °C and 514 °C. The weight loss of 12% is concluded upon heating from 514 °C to 775 °C, indicating the final decomposition of carbon residues. On the other hand, the evolution of gases in EGA curves shows two main characteristic steps in the decomposition: the first step consists of simultaneous detection of H_2O and CO_2, indicating the thermal oxidation of CH-groups from 217 °C to 514 °C, and the second step is the evolution of only CO_2 gas indicating the decomposition of carbonate groups in the interval 580 °C to 775 °C where the last CO_2 peak is recorded. For comparison, the thermal decompositions of 2-methoxyethanol-acetic acid- and 1-methoxy-2-propanol-acetic acid-based gels were concluded at about 150 °C and 246 °C higher temperatures, at 924 °C and 1021 °C, respectively.[32]

Fig. 3 shows the XRD pattern of the BZT–BCT xerogel calcined at 900 °C for 30 minutes demonstrating that the sample crystallizes in the perovskite phase. The result supports the thermal analysis data.

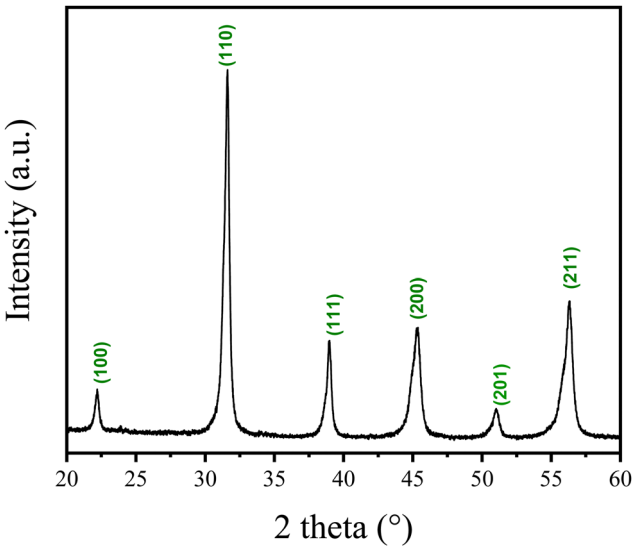

Fig. 3 XRD pattern of BZT–BCT xerogel calcined at 900 °C. The peaks are indexed according to PDF 01-074-4539 (BT cubic phase).

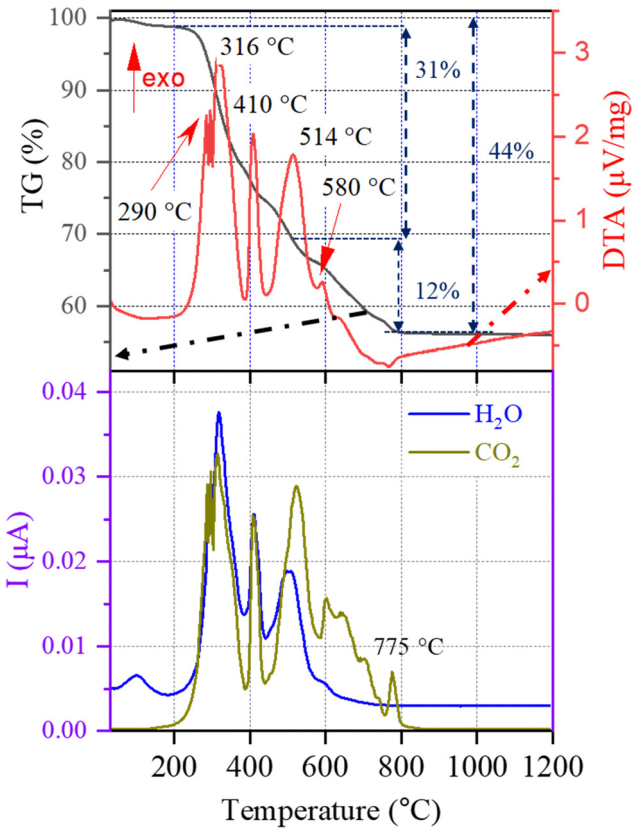

Fig. 2 Thermal decomposition of the BZT–BCT xerogel in synthetic air followed by TG, DTA and EGA (H_2O and CO_2). I: ion current.

The FTIR spectra of 0.2M-2min and 0.2M-15min films were recorded after the pyrolysis and RTA steps at 500 °C, 600 °C, 700 °C, 750 °C and 800 °C and are shown in Fig. 4(a) and (b), respectively. The thickness of such one-layer films is estimated to be a few tens of nanometers. In 0.2M-2min and 0.2M-15min films heated at 350 °C and at 500 °C, the acetate groups are identified by the absorption bands at about 1428 cm^{-1} and 1571 cm^{-1} for (COO^-) symmetric and (COO^-) asymmetric stretching vibrations. The obvious band of the carbonate groups is recorded at 1446 cm^{-1} in both films upon heating to 600 °C which agrees with the EGA data (*cf.* Fig. 2). At 750 °C, the carbonate groups are almost fully decomposed in the 0.2M-15min film while their presence is evident in the 0.2M-2min film. In both films, the metal–oxygen (M–O) band is evident at/above 750 °C. This reveals that the drying and pyrolysis times influence the decomposition process of organic residues and could affect the microstructure.

Fig. 5 shows the time-of-flight secondary ion mass spectrometry (ToF-SIMS) analysis of 0.2M-2min and 0.2M-15min films annealed at 500 °C, 600 °C and 750 °C. The detection of carbonate ions during the sputtering reveals that up to 500 °C, there is almost no formation of carbonates in both 0.2M-2min and 0.2M-15min films, see Fig. 5(a) and (d). Note that the signals at the beginning of sputtering are due to the contamination of the sample surface. At 600 °C a significant amount of carbonate ions is identified. Although the analysis is not quantitative, the same secondary ions can be compared between each other since we have very similar composition of the samples. From the intensity ratios of carbonate CO_3^- ions to the intensity of BaO_2^- ions, it is obvious that the 0.2M-2min film contains more carbonaceous residues than the 0.2M-15min film at the same temperature; compare Fig. 5(b) and (e). This difference is attributed to insufficient drying and pyrolysis times

Open Access Article. Published on 08 August 2024. Downloaded on 10/19/2025 2:20:13 PM.
This article is licensed under a Creative Commons Attribution 3.0 Unported Licence.

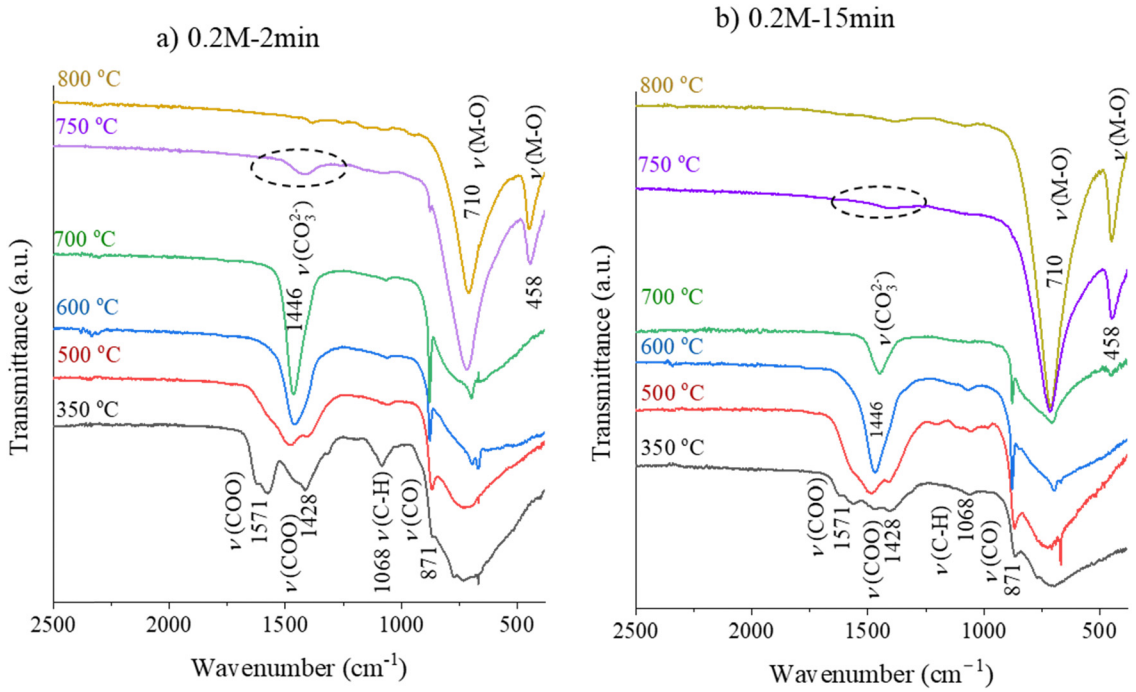

Fig. 4 FTIR spectra of the (a) 0.2M-2min and (b) 0.2M-15min films heated at different temperatures for 6 seconds.

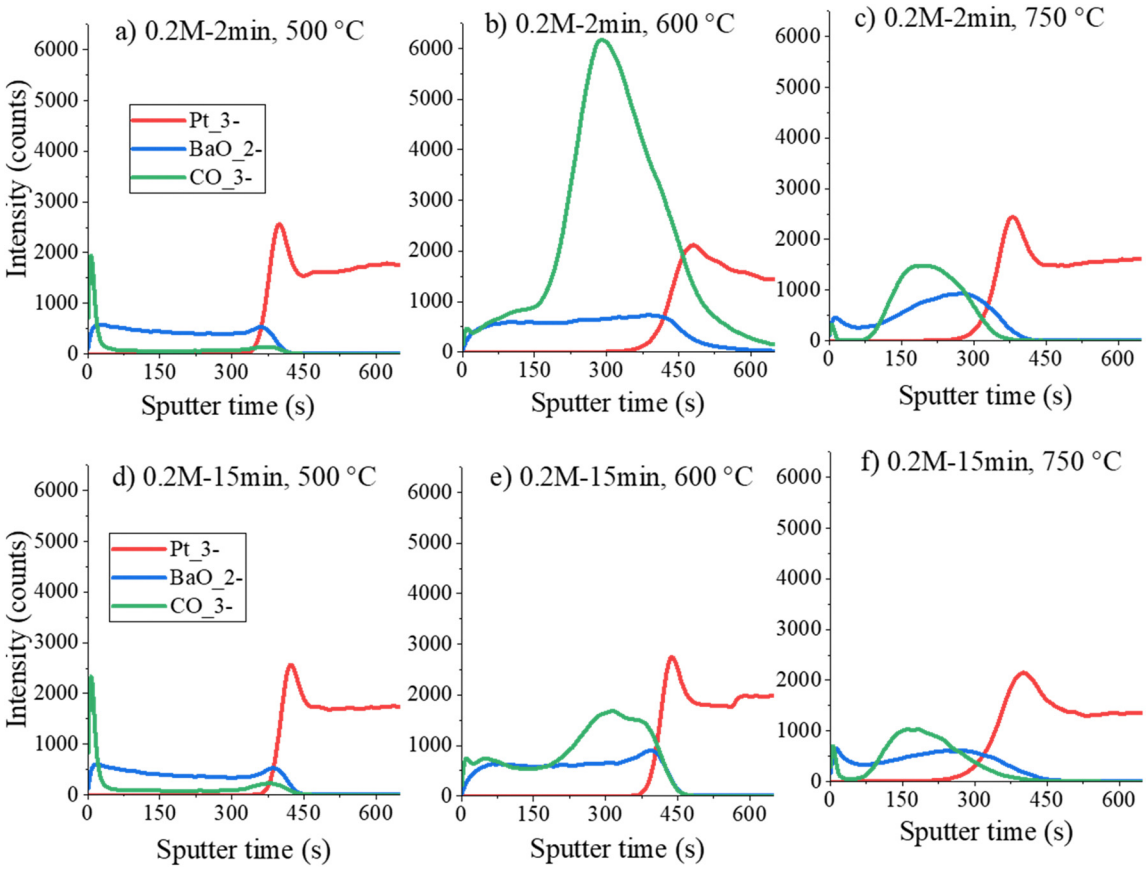

Fig. 5 ToF-SIMS depth profiles of (a)–(c) 0.2M-2min films and (d)–(f) 0.2M-15min films heated at 500 °C, 600 °C and 750 °C.

 This journal is © The Royal Society of Chemistry 2024

Open Access Article. Published on 08 August 2024. Downloaded on 10/19/2025 2:20:13 PM.
This article is licensed under a Creative Commons Attribution 3.0 Unported Licence.

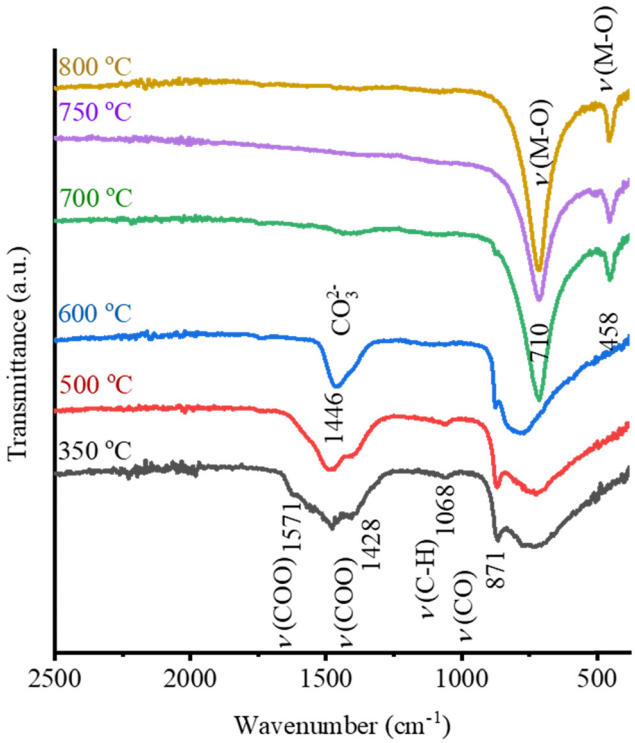

Fig. 6 FTIR spectra of 0.1M-15min film annealed at different temperatures for 6 seconds.

to oxidize the major carbon residues. In both cases, the ToF-SIMS analysis agrees with the FTIR and thermal analysis results that the carbonates are predominantly formed upon annealing at 600 °C. Upon annealing at 750 °C, up to the depth of approximately 5 nm (0 to 60 seconds of sputtering in Fig. 5(c) and (f)), some carbonate species are still present deeper in the film. This suggests that upon heating in an RTA furnace, the carbonates are decomposed starting from the top of the films, leading to the inference that the thinner the film is, the faster the carbonate groups will be decomposed. The broadening of the interfaces between the films and the Pt-layer (curves for BaO_2/Pt_3) in the SIMS depth profiles in Fig. 5 is due to an artifact related to the ion bombardment during SIMS depth profiling.

The concentration of the BZT–BCT coating solution was found to influence the films' microstructure. When processed at the same drying/pyrolysis/annealing conditions, the BZT–BCT films deposited from 0.2 M or 0.1 M solutions have granular or columnar microstructures, respectively.[28] We used FTIR to follow the thermal decomposition of the 0.1M-15min films to see if there was any difference in the thermal decomposition pathways of the films prepared from 0.1 M and 0.2 M solutions.

The FTIR spectra of the 0.1M-15min films are shown in Fig. 6. The band of the carbonate groups is present in the film annealed at 600 °C while it almost disappears in the film annealed at 700 °C. In this latter spectrum the M–O bands at 710 cm^{-1} and 458 cm^{-1} are recorded, indicating the oxide formation. Note that in the case of 0.2M-15min films, such a FTIR spectrum is observed only upon annealing at 750 °C, as shown in Fig. 4b. The influence of the concentration of the coating solution on the thin film crystallization is not surprising since it has been reported that by decreasing the coating solution concentration and thus reducing the individual layer thickness, columnar grains can be achieved in BT, $SrTiO_3$, and (Ba, Sr)TiO_3 films.[33–36]

By repeating the spin-coating 0.2 M or 0.1 M solutions, drying, pyrolysis and RTA steps 4 or 10 times, we prepared the films at the final temperatures of 600, 700, 800 and 850 °C. The phase composition of respective films is shown in Fig. 7.

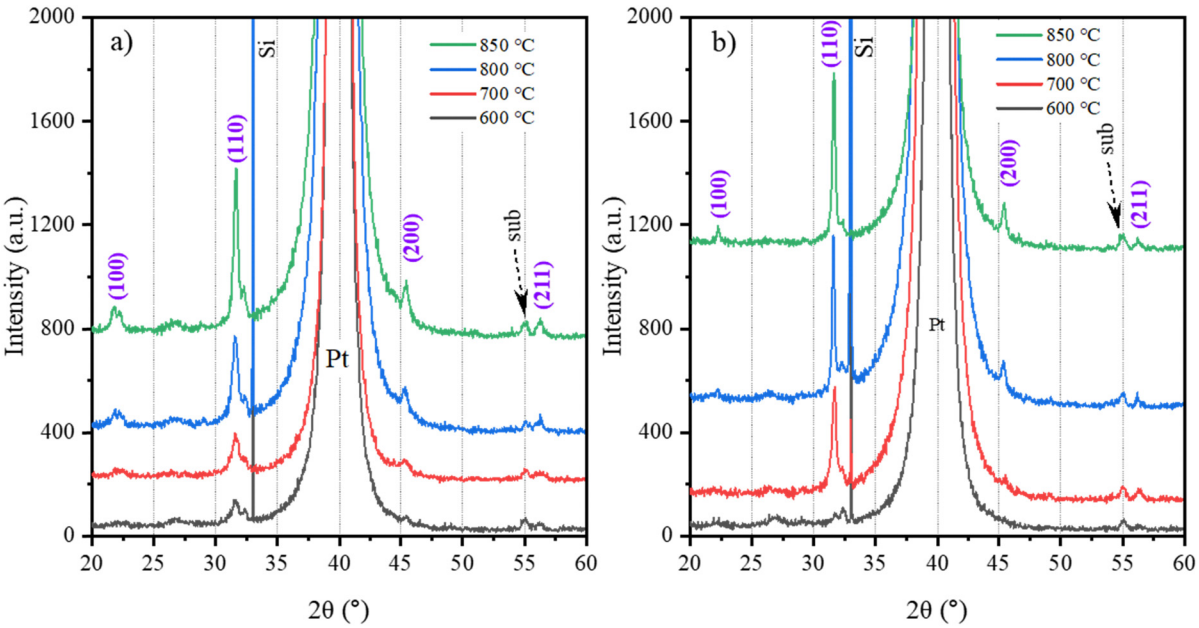

Fig. 7 XRD patterns of (a) 0.2M-600, 0.2M-700, 0.2M-800, and 0.1M-850 thin films and (b) 0.1M-600, 0.1M-700, 0.1M-800, and 0.1M-850 thin films.

Open Access Article. Published on 08 August 2024. Downloaded on 10/19/2025 2:20:13 PM.
This article is licensed under a Creative Commons Attribution 3.0 Unported Licence.

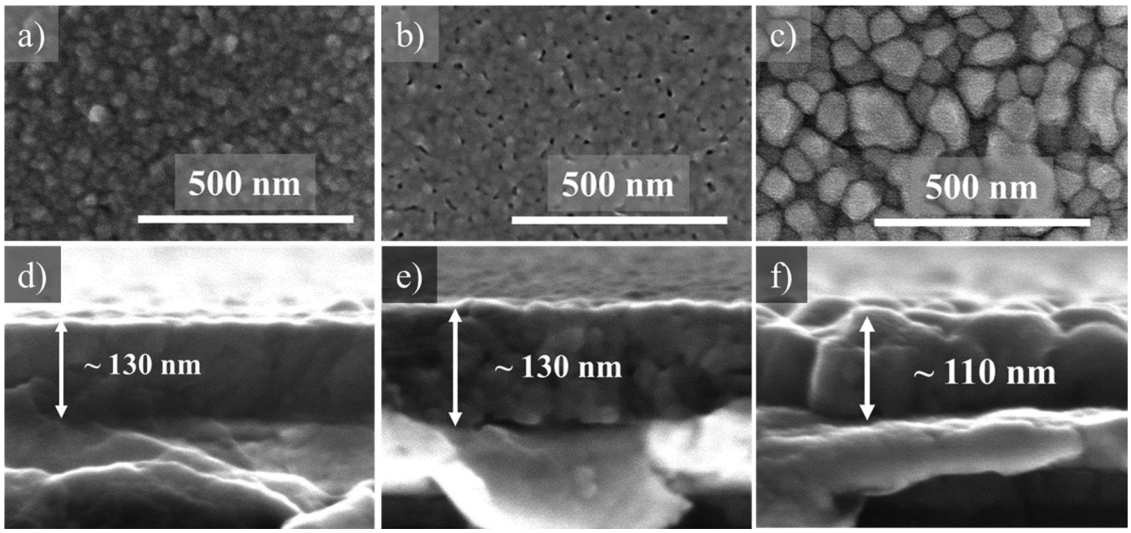

Fig. 8 SEM (a)–(c) plan view micrographs of 0.1M-700, 0.1M-800 and 0.1M-850 films and (d)–(f) their respective cross-sections.

In both 0.2M-600 and 0.1M-600 films, weak (110) and (211) peaks are observed, indicating the onset of crystallization. With increasing temperature, the intensity of the (110) peak increases, indicating that a higher crystallinity and also lower-intensity perovskite reflections emerge. Note that the perovskite (111) peak cannot be distinguished as it coincides with the Pt(111) peak. The intensity of the perovskite peaks in 0.1M-700, 0.1M-800, and 0.1M-850 films is stronger compared to the 0.2M-700, 0.2M-800, and 0.2M-850 films indicating higher crystallinity in the former group.

In our previous study, we prepared BZT–BCT films from the 0.2 M solution and annealed them at 800, 850, and 900 °C. All films had porous microstructures consisting of fine equiaxed grains.[30] We analyzed the microstructure of 0.1M-700, 0.1M-800, and 0.1M-850 thin films by using scanning electron microscopy, see Fig. 8. The surface microstructures of the films annealed at 700 °C and 800 °C are porous with fine grains of a few 10 nm. The film thickness is about 130 nm. The surface microstructure of the film annealed at 850 °C is dense, with grains ranging from 60 to 100 nm. The cross-section micrograph reveals columnar grains extending through the film thickness. The film thickness is about 110 nm, indicating densification at this temperature.

We selected 0.1M-850 films to investigate the distribution of the elements using XPS depth profiling across the area with a diameter of 400 μm. The spectrum shown in Fig. 9 reveals that

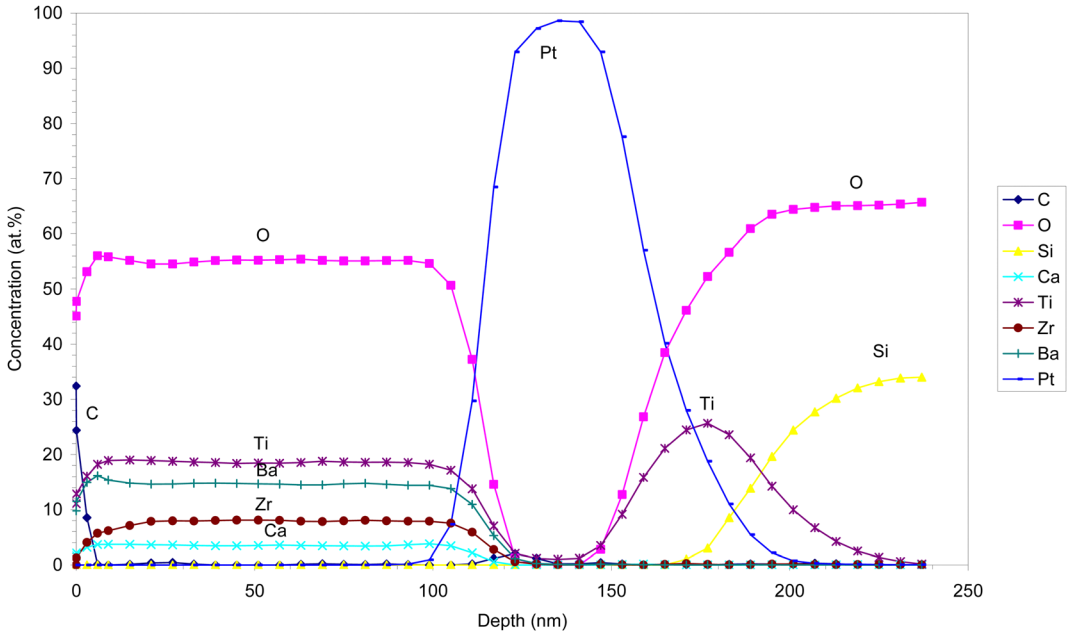

Fig. 9 XPS depth profile of the 0.1M-850 film.

 This journal is © The Royal Society of Chemistry 2024

Open Access Article. Published on 08 August 2024. Downloaded on 10/19/2025 2:20:13 PM.
This article is licensed under a Creative Commons Attribution 3.0 Unported Licence.

the film consists of Ba, Ca, Ti, Zr, and O with a thickness of about 110 nm. The film's surface is covered with a carbon-rich layer of 2 nm, probably due to contamination. The distribution of the elements throughout the film thickness is uniform. This indicates that the crystallization from the amorphous phase within each deposited BZT–BCT layer occurs without any change in chemical composition or segregation, as is the case in the crystallization of PZT thin films.[37] The interface with the $Pt/TiO_2/SiO_2$ substrate is sharp, indicating that there is no chemical interaction between the film and the substrate.

We note that in our previous study, the manganese-doped BZT–BCT film annealed at 850 °C with a columnar microstructure was analyzed by using scanning transmission electron microscopy (STEM) and energy dispersive X-ray spectroscopy (EDS). A homogeneous distribution of elements within one columnar grain across the film thickness was observed. Mn-dopant was added to BZT–BCT to reduce the leakage current, and its addition did not influence the crystallization and microstructure.[30] The results of STEM-EDS analysis are in a very good agreement with the XPS analysis, confirming that chemical homogeneity in the BZT–BCT films is achieved not only within individual grains but also across the area of about 0.1 mm^2.

Conclusions

The thermal processing of $0.5Ba(Ti_{0.8}Zr_{0.2})O_3$–$0.5(Ba_{0.7}Ca_{0.3})TiO_3$ (BZT–BCT) thin films from ethylene glycol-based precursor solution and the homogeneity of the crystalline films on a platinized silicon substrate were studied. Prolonging the drying and pyrolysis times from 2 minutes to 15 minutes of the one-layer films deposited from a 0.2 M solution contributes to the completion of the thermal decomposition of carbon residues at a lower temperature. By decreasing the concentration of the coating solution from 0.2 M to 0.1 M, or in other words, by reducing the deposited layer thickness to about 10 nm, the thermal decomposition of carbonate groups is significantly downshifted. Both approaches, extended drying and pyrolysis times and reducing the coating solution concentration, contribute to the perovskite crystallization at about 700 °C. Still, to obtain a dense columnar microstructure of BZT–BCT films, multi-step annealing at 850 °C was needed. Depth profiling revealed a homogeneous distribution of constituent elements across the thickness of the film. Our results show that processing optimization in the microstructure engineering of BZT–BCT thin films is key to optimizing their functional properties.

Author contributions

Conceptualization, S. W. K. and B. M.; methodology, B. M., S. W. K.: chemical solution deposition of thin films, FTIR analysis, XRD analysis, S. W. K.; thermal analysis, S. W. K., B. M.; SEM: K. Ž.; ToF-SIMS, XPS: J. E., J. K.; resources, B. M.; writing – original draft preparation, S. W. K. and B. M.; writing – review and editing, all authors; supervision, B. M.; funding acquisition, B. M., and J. K. All authors have read and agreed to the published version of the manuscript.

Data availability

No primary research results, software or code have been included and no new data were generated or analysed as part of this article.

Conflicts of interest

There are no conflicts to declare.

Acknowledgements

We thank Jana Cilenšek for performing the thermal analysis of xerogels. The authors acknowledge the financial support from the Slovenian Research and Innovation Agency (core funding P2-0105 and P2-0082, S. W. K., K. Ž., and J. E.: national postgraduate research funding).

References

1 W. Liu and X. Ren, Large piezoelectric effect in Pb-free ceramics, *Phys. Rev. Lett.*, 2009, **103**(25), 257602, DOI: 10.1103/PhysRevLett.103.257602.
2 M. Acosta, N. Novak, G. A. Rossetti and J. Rödel, Mechanisms of electromechanical response in $(1-x)$ $Ba(Zr_{0.2}Ti_{0.8})O_{3-x}$ $(Ba_{0.7}Ca_{0.3})TiO_3$ ceramics, *Appl. Phys. Lett.*, 2015, **107**(14), 142906, DOI: 10.1063/1.4932654.
3 J. Gao, D. Xue, W. Liu, C. Zhou and X. Ren, Recent progress on $BaTiO_3$-based piezoelectric ceramics for actuator applications, *Actuators*, 2017, **6**(3), 24, DOI: 10.3390/act6030024.
4 J. Rödel, K. G. Webber, R. Dittmer, W. Jo, M. Kimura and D. Damjanovic, Transferring lead-free piezoelectric ceramics into application, *J. Eur. Ceram. Soc.*, 2015, **35**(6), 1659–1681, DOI: 10.1016/j.jeurceramsoc.2014.12.013.
5 D. S. Keeble, F. Benabdallah, P. A. Thomas, M. Maglione and J. Kreisel, Revised structural phase diagram of $(Ba_{0.7}Ca_{0.3}TiO_3)$–$(BaZr_{0.2}Ti_{0.8}O_3)$, *Appl. Phys. Lett.*, 2013, **102**(9), 092903, DOI: 10.1063/1.4793400.
6 J. Gao, X. Ke, M. Acosta, J. Glaum and X. Ren, High piezoelectricity by multiphase coexisting point: Barium titanate derivatives, *MRS Bull.*, 2018, **43**(8), 595–599, DOI: 10.1557/mrs.2018.155.
7 M. C. Ehmke, S. N. Ehrlich, J. E. Blendell and K. J. Bowman, Phase coexistence and ferroelastic texture in high strain $(1-x)$ Ba $(Zr_{0.2}Ti_{0.8})O_{3-x}$ $(Ba_{0.7}Ca_{0.3})TiO_3$ piezoceramics, *J. Appl. Phys.*, 2012, **111**(12), 124110, DOI: 10.1063/1.4730342.
8 L. Zhang, M. Zhang, L. Wang, C. Zhou, Z. Zhang, Y. Yao and X. Ren, Phase transitions and the piezoelectricity around morphotropic phase boundary in $Ba(Zr_{0.2}Ti_{0.8})O_{3-x}$ $(Ba_{0.7}Ca_{0.3})TiO_3$ lead-free solid solution, *Appl. Phys. Lett.*, 2014, **105**(16), 162908, DOI: 10.1063/1.4899125.
9 M. Maraj, W. Wei, B. Peng and W. Sun, Dielectric and energy storage properties of $Ba(1-x)Ca_xZr_yTi_{(1-y)}O_3$ (BCZT): a review, *Materials*, 2019, **12**(21), 3641, DOI: 10.3390/ma12213641.

Open Access Article. Published on 08 August 2024. Downloaded on 10/19/2025 2:20:13 PM.
This article is licensed under a Creative Commons Attribution 3.0 Unported Licence.

10 C.-B. Eom and S. Trolier-McKinstry, Thin-film piezoelectric MEMS, *MRS Bull.*, 2012, **37**(11), 1007–1017, DOI: 10.1557/mrs.2012.273.

11 K. L. Ekinci and M. L. Roukes, Nanoelectromechanical systems, *Rev. Sci. Instrum.*, 2005, **76**(6), 061101, DOI: 10.1063/1.1927327.

12 U. Hasenkox, S. Hoffmann and R. Waser, Influence of precursor chemistry on the formation of $MTiO_3$ (M= Ba, Sr) ceramic thin films, *J. Sol-Gel Sci. Technol.*, 1998, **12**, 67–79, DOI: 10.1023/A:1026480027046.

13 H. S. Gopalakrishnamurthy, M. S. Rao and T. N. Kutty, Thermal decomposition of titanyl oxalates I: Barium titanyl oxalate, *J. Inorg. Nucl. Chem.*, 1975, **37**(4), 891–898, DOI: 10.1016/0022-1902(75)80668-3.

14 O. A. Harizanov, Formation and crystallization of an acetate-acetylacetonate derived sol–gel $BaTiO_3$, *Mater. Lett.*, 1998, **34**(3–6), 345–350, DOI: 10.1016/S0167-577X(97)00199-7.

15 S. M. Aygün, P. Daniels, W. J. Borland and J. P. Maria, In situ methods to explore microstructure evolution in chemically derived oxide thin films, *J. Mater. Res.*, 2010, **25**(3), 427–436.

16 T. Dechakupt, G. Yang, C. A. Randall, S. Trolier-McKinstry and I. M. Reaney, Chemical Solution-Deposited BaTiO3 Thin Films on Ni Foils: Microstructure and Interfaces, *J. Am. Ceram. Soc.*, 2008, **91**(6), 1845–1850, DOI: 10.1111/j.1551-2916.2008.02407.x.

17 S. W. Konsago, K. Žiberna, B. Kmet, A. Benčan, H. Uršič and B. Malič, Chemical Solution Deposition of Barium Titanate Thin Films with Ethylene Glycol as Solvent for Barium Acetate, *Molecules*, 2022, **27**(12), 3753, DOI: 10.3390/molecules27123753.

18 M. Bilton, A. P. Brown and S. J. Milne, Investigating the optimum conditions for the formation of calcium oxide, used for CO_2 sequestration, by thermal decomposition of calcium acetate, *J. Phys.: Conf. Ser.*, 2012, **371**(1), 012075, DOI: 10.1088/1742-6596/371/1/012075.

19 K. S. Karunadasa, C. H. Manoratne, H. M. T. G. A. Pitawala and R. M. G. Rajapakse, Thermal decomposition of calcium carbonate (calcite polymorph) as examined by *in situ* high-temperature X-ray powder diffraction, *J. Phys. Chem. Solids*, 2019, **134**, 21–28, DOI: 10.1016/j.jpcs.2019.05.023.

20 D. Van den Eynden, R. Pokratath and J. De Roo, Nonaqueous Chemistry of Group 4 Oxo Clusters and Colloidal Metal Oxide Nanocrystals, *Chem. Rev.*, 2022, **122**(11), 10538–10572, DOI: 10.1021/acs.chemrev.1c01008.

21 C. J. Brinker and G. W. Scherer, *Sol-gel science: the physics and chemistry of sol-gel processing*, Academic Press, San Diego, 1990, pp. 52–59.

22 F. Babonneau, S. Doeuff, A. Leaustic, C. Sanchez, C. Cartier and M. Verdaguer, XANES and EXAFS study of titanium alkoxides, *Inorg. Chem.*, 1988, **27**(18), 3166–3172, DOI: 10.1021/ic00291a024.

23 D. Peter, T. S. Ertel and H. Bertagnolli, EXAFS study of zirconium alkoxides as precursor in the sol-gel process: I. Structure investigation of the pure alkoxides, *J. Sol-Gel Sci. Technol.*, 1994, **3**, 91–99, DOI: 10.1007/BF00486715.

24 H. Wang, J. Xu, C. Ma, F. Xu, L. Wang, L. Bian and A. Chang, Spectroscopic ellipsometry study of $0.5BaZr_{0.2}Ti_{0.8}O_3$ – $0.5Ba_{0.7}Ca_{0.3}TiO_3$ ferroelectric thin films, *J. Alloys Compd.*, 2014, **615**, 526–530, DOI: 10.1016/j.jallcom.2014.06.186.

25 P. S. Barbato, V. Casuscelli, P. Aprea, R. Scaldaferri and D. Caputo, Optimization of the production process of BZT–BCT sol–gel thin films obtained from a highly stable and green precursor solution, *Mater. Manuf. Processes*, 2021, **36**(14), 1642–1649, DOI: 10.1080/10426914.2021.1926495.

26 Z. Wang, Z. Cai, H. Wang, Z. Cheng, J. Chen, X. Guo and H. Kimura, Lead-free $0.5Ba(Ti_{0.8}Zr_{0.2})O_{3-0.5}(Ba_{0.7}Ca_{0.3})TiO_3$ thin films with enhanced electric properties fabricated from optimized sol-gel systems, *Mater. Chem. Phys.*, 2017, **186**, 528–533, DOI: 10.1016/j.matchemphys.2016.11.030.

27 G. Kang, K. Yao and J. Wang, $(1-x)$ $Ba(Zr_{0.2}Ti_{0.8})O_{3-x}$ $(Ba_{0.7}Ca_{0.3})TiO_3$ Ferroelectric Thin Films Prepared from Chemical Solutions, *J. Am. Ceram. Soc.*, 2012, **95**(3), 986–991, DOI: 10.1111/j.1551-2916.2011.04877.x.

28 Z. L. Cai, Z. M. Wang, H. H. Wang, Z. X. Cheng, B. W. Li, X. L. Guo and A. Kasahara, An Investigation of the Nanomechanical Properties of 0.5 $Ba(Ti_{0.8}Zr_{0.2})O_{3-0.5}$ $(Ba_{0.7}Ca_{0.3})TiO_3$ Thin Films, *J. Am. Ceram. Soc.*, 2015, **98**(1), 114–118, DOI: 10.1111/jace.13228.

29 J. Xu, Y. Zhou, Z. Li, C. Lin, X. Zheng, T. Lin and F. Wang, Microstructural, ferroelectric and photoluminescence properties of Er^{3+}-doped $Ba_{0.85}Ca_{0.15}Ti_{0.9}Zr_{0.1}O_3$ thin films, *Mater. Chem. Phys.*, 2021, **262**, 124320, DOI: 10.1016/j.matchemphys.2021.124320.

30 S. W. Konsago, K. Žiberna, A. Matavž, B. Mandal, S. Glinšek, Y. Fleming, A. Benčan, L. G. Brennecka, H. Uršič and B. Malič, Engineering the Microstructure and Functional Properties of $0.5Ba(Zr_{0.2}Ti_{0.8})O_{3-05}(Ba_{0.7}Ca_{0.3})TiO_3$ Thin Films, *ACS Appl. Electron. Mater.*, 2024, **6**(6), 4467–4477, DOI: 10.1021/acsaelm.4c00530.

31 F. J. Moulder, W. F. Stickle, P. E. Sobol and K. D. Bomben, *X-ray photoelectron spectroscopy: A reference book of standard spectra for identification and interpretation of XPS data*, Physical Electronics Division, PerkinElmer Corporation, Eden Prairie, Minnesota, 1992.

32 P. S. Barbatoa, V. Casuscellib, P. Apreaa, R. Scaldaferrib, I. Pedacib and D. Caputoa, Green production of lead-free bzt-bct thin films for applications in mems devices, *Chem. Eng. Trans.*, 2021, **84**, 97–102, DOI: 10.3303/CET2184017.

33 S. Hoffmann, U. Hasenkox, R. Waser, C. L. Jia and K. Urban, Chemical Solution Deposited $BaTiO_3$ and $SrTiO_3$ Thin Films with Columnar Microstructure, *MRS Online Proc. Libr.*, 1997, **474**, 9, DOI: 10.1557/PROC-474-9.

34 S. Hoffmann and R. Waser, Control of the morphology of CSD-prepared $(Ba,Sr)TiO_3$ thin films, *J. Eur. Ceram. Soc.*, 1999, **19**(6–7), 1339–1343, DOI: 10.1016/S0955-2219(98)00430-0.

35 C. Mansour, M. Benwadih and C. Revenant, Sol–gel derived barium strontium titanate thin films using a highly diluted precursor solution, *AIP Adv.*, 2021, **11**(8), 085302, DOI: 10.1063/5.0055584.

36 J. F. Ihlefeld, A. M. Vodnick, S. P. Baker, W. J. Borland and J. P. Maria, Extrinsic scaling effects on the dielectric response of ferroelectric thin films, *J. Appl. Phys.*, 2008, **103**(7), 074112, DOI: 10.1063/1.2903211.

37 F. Calame and P. Muralt, Growth and properties of gradient free sol-gel lead zirconate titanate thin films, *Appl. Phys. Lett.*, 2007, **90**(6), 062907, DOI: 10.1063/1.2472529.

 This journal is © The Royal Society of Chemistry 2024